Electronic Supplementary Material (ESI) for Materials Horizons.
This journal is © The Royal Society of Chemistry 2024

Supporting Information

Rapid synthesis of high-purity molybdenum carbide with controlled crystal phases

Renjie Fang, Haoxian He, Zhiyi Wang, Ye-Chuang Han and Feng Ru Fan**

State Key Laboratory of Physical Chemistry of Solid Surfaces, College of Chemistry and Chemical Engineering, Innovation Laboratory for Sciences and Technologies of Energy Materials of Fujian Province (IKKEM), Xiamen University, Xiamen 361005, China.

Materials and methods

Materials

Ammonium paramolybdate (APM, $(NH_4)_6Mo_7O_{24}\cdot 4H_2O$, AR) and 4-Cl-o-phenylenediamine (4Cl-oPDA, 97%) were purchased from Shanghai Aladdin Biochemical Technology Co., Ltd. Hydrochloric acid (AR), sulfuric acid (AR), ethanol (AR), and ethyl alcohol (AR) were purchased from Sinopharm Chemical Reagent Co., Ltd. Nafion (5%) was purchased from Du Pont China Holding Co., Ltd. Chloroplatinic acid hexahydrate ($H_2Cl_6Pt\cdot 6H_2O$, 99.995%) and 20% Pt/C was purchased from Shanghai Macklin Biochemical Co., Ltd. Carbon cloth (CC) and conductive carbon paper were purchased from Ce Tech Co., Ltd. Carbon black (VULCANXC72R) was purchased from Cabot Co., Ltd. N_2 (99.999%) and H_2 (99.999%) were purchased from Linde Industrial Gases. Deionized water was used throughout.

Synthesis of MoO_x/4-Cl-o-phenylenediamine hybrid

The MoO_x/4-Cl-o-phenylenediamine hybrid precursors were prepared as follows: First, ammonium paramolybdate (APM, 1.0 g) and 4-Cl-o-phenylenediamine (4Cl-oPDA, 2.76 g) were dissolved in deionized water (60 mL). Then, the pH of the solution was adjusted to 1.0-2.0 using 1 M HCl which caused the amine-oxide hybrid to precipitate. Next, the solution was heated to 50 °C with stirring for 3 h. The precipitate was then collected by centrifugation at 8000 RPM for 3 min, and washed with deionized water and ethanol. Finally, the amine-oxide hybrid was obtained after drying at 60 °C.

Synthesis of molybdenum carbides

First, MoO_x/4Cl-oPDA hybrid (50 mg) was pressed into a pellet (diameter of 8 mm for synthesizing β-Mo_2C and η-MoC_{1-x}, diameter of 6 mm for synthesizing α-MoC_{1-x}) under a pressure of 8 MPa, and the pellet was immobilized into two layers of CC (33 mm in length and

10 mm in width for synthesizing β-Mo_2C and η-MoC_{1-x}, 33 mm in length and 8 mm in width for synthesizing α-MoC_{1-x}). Then, the CC-held hybrid pellet was placed into a homemade carbon heater in N_2, and the two sides of the CC were connected with a copper electrode. In a typical heating program, the electrical power applied to the carbon heater was switched from the 'off' state to the 'on' state and held for 0.6 s to carry out the carbothermal reduction, followed by removing the power to turn the heater back off for 5 s to complete a period of 5.6 s, which is then repeated 150 cycles. The set temperature was achieved by regulating the output electric current. Molybdenum carbides including thermodynamically stable β-Mo_2C, and metastable α-MoC_{1-x} and η-MoC_{1-x} were selectively synthesized by adjusting the output electric current, discharge time and the number of repetitions. MoO_x/4Cl-oPDA hybrid (500 mg) was annealed in a tube furnace under Argon at 850 °C for 12 h to form β-$Mo_2C_{(TPR)}$. APM (1.0 g) was physically mixed with 4Cl-oPDA (2.76 g) by manual pestle grinding for 10 min. Then, the mixture (50 mg) was pressed into a pellet and products were collected as the control by a typical PJH program.

Molybdenum carbide supported Pt synthesis

Pt was deposited onto molybdenum carbide (2 wt%) using an incipient wetness impregnation (IWI) method. $H_2PtCl_6 \cdot 6H_2O$ solution (100 mL, 10.84 mg/mL) was finely mixed with molybdenum carbide (20 mg), followed by drying in a vacuum oven at 80 °C after 20 minutes of ultrasound. Molybdenum carbide supported Pt was reduced in 10% H_2/N_2 flow with a temperature ramping rate of 20 °C min^{-1} up to 400 °C and kept at 400 °C for 30 min.

2 wt% Pt/C is also synthesized as a contrast using carbon black by IWI method.

Hydrogen evolution reaction (HER) test

The binder solution was prepared by mixing 5 wt% Nafion solution (20 μL) with ethyl alcohol (480 μL) and Deionized water (500 μL). The catalyst ink was then prepared by dispersion of molybdenum carbides (5 mg) into 1 mL binder solution followed by ultrasonication for 30 min. The ink (20 μL) was then deposited onto a conductive carbon paper (1 cm×1 cm, catalyst loading ~100 μg cm^{-2}) and dried in the air as the working electrode. Electrochemical measurements were conducted using a CHI 660E electrochemical workstation in a 0.5 M H_2SO_4 solution. The standard three-electrode setup was applied, where a silver chloride electrode (SCE) was used as the reference, the catalyst-loaded conductive carbon paper was used as the working electrode, and a graphite rod was used as the counter electrode. Linear sweep voltammetry (LSV) was carried out at a scan rate of 5 mV s^{-1}, while the stability of the catalysts was studied at a fast scan rate (100 mV s^{-1}) for 1000 cycles.

Oxygen reduction reaction (ORR) test

The binder solution was prepared by mixing 5 wt% Nafion solution (20 μL) with ethyl alcohol (480 μL) and Deionized water (500 μL). The catalyst ink was then prepared by dispersion of molybdenum carbides (5 mg) into 1 mL binder solution followed by ultrasonication for 30 min. The ink (10 μL) was then deposited onto a glassy carbon electrode with a diameter of 5 mm (catalyst loading ~254.8 μg cm^{-2}) and dried in the air as the working electrode. Electrochemical measurements were conducted using a CHI 660E electrochemical workstation in a 0.1 M KOH solution using a rotating disk electrode (RDE) technique. The standard three-electrode setup was applied, where a silver chloride electrode (SCE) was used as the reference, the catalyst-loaded glassy carbon electrode was used as the working electrode, and a graphite rod was used as the counter electrode. Linear sweep voltammetry (LSV) was carried out at a scan rate of 5 mV s^{-1}

with a rotating speeds of 1600 rpm to evaluate the electrocatalytic ORR activity of the synthesized material.

Double-layer capacitance (C_{dl}) measurement

To measure the double-layer capacitance (C_{dl}), cyclic voltammetry (CV) experiments were conducted in 0.5M H_2SO_4 electrolyte solution at room temperature. The experiments were performed using a three-electrode system, with a graphite rod as the counter electrode, a saturated calomel electrode (SCE) as the reference electrode, and the test material as the working electrode. The scan rates varied from 20 to 120 mV/s to ensure a broad evaluation of capacitive behaviors, and the voltage range was limited to a non-Faradaic region where no redox reactions occur, to isolate the capacitive response of the material.

The ECSA was calculate by the following formula:

$$ECSA = \frac{C_{measured}}{C_{specific}}$$

Here, $C_{measured}$ is the measured double layer capacitance value, $C_{specific}$ is a double layer permittivity per unit surface area, and is typically about 20 μF/cm² (for a perfectly smooth metal surface in contact with an electrolyte solution of ordinary concentration).[1]

Table S1. Parameters for molybdenum carbides synthesis.

Precursors	Mass (mg)	Pellet diameter (mm)	Current (A)	Pulse time (s)	Pulse cycles	Carbon cloth width (mm)	Heating rate (K/s)	Product
MoO_x/4-Cl-o-phenylenediamine hybrid	50	8	30	0.6	2	10	1160	α-MoC_{1-x}
	50	6	30	1.5	1	8	2360	α-MoC_{1-x} (better crystallinity)
	50	8	30	0.6	16	10	1160	η-MoC_{1-x}
	50	8	34	2.4	4	10	1570	η-MoC_{1-x} (better crystallinity)
	50	8	30	0.6	150	10	1160	β-Mo_2C

Table S2. Elemental analysis result of MoO_x/4-Cl-o-phenylenediamine hybrid measured by energy dispersive spectroscopy (EDS) mapping.

Element	Content (wt%)	Content (at%)
Mo	40.17	9.00
C	29.76	53.31
O	19.02	25.56
N	5.84	8.97
Cl	5.22	3.16

Table S3. Pt content in Pt doped molybdenum carbides measured by ICP-OES.

Catalyst	Pt content (wt%)
2% Pt/α-MoC_{1-x}	0.71
2% Pt/η-MoC_{1-x}	0.70
2% Pt/β-Mo_2C	0.73
2% Pt/C	0.73

Table S4. C_{dl} and ECSA of the Pt-based catalysts.

Catalyst	C_{dl} (mF cm^{-2})	ECSA (cm^2)
2% Pt/C	2.01	100.5
2% Pt/α-MoC_{1-x}	0.64	32
2% Pt/η-MoC_{1-x}	0.52	26
2% Pt/β-Mo_2C	0.39	19.5

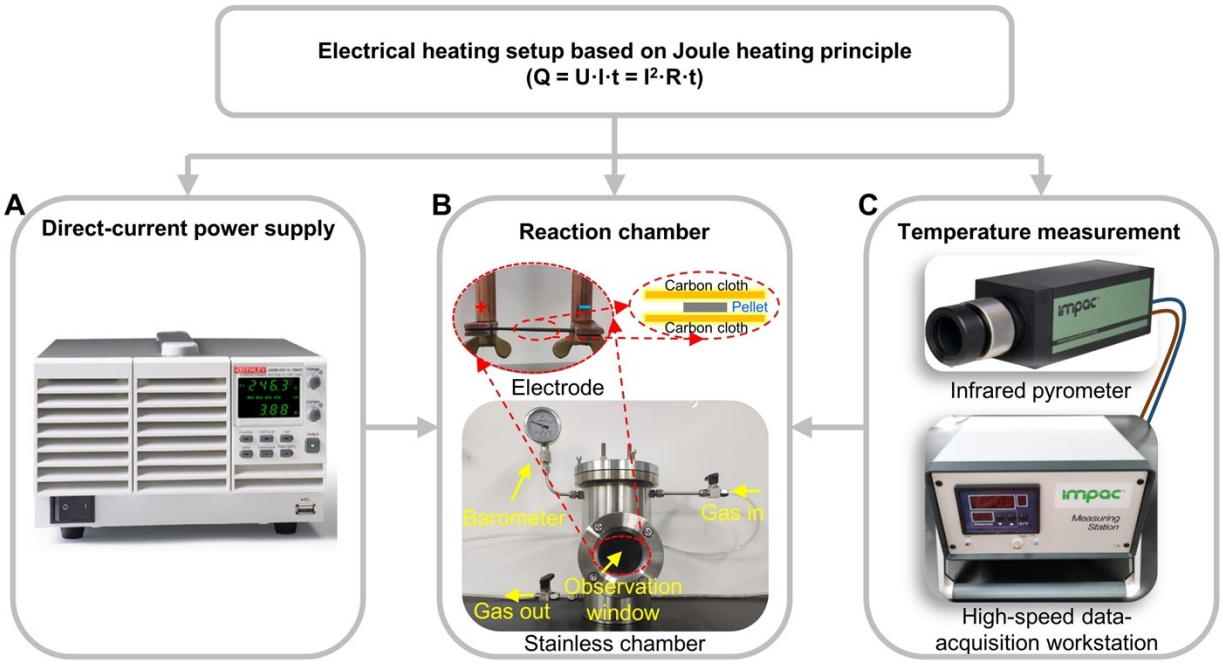

Figure S1. Electrical heating setup. (**a**) Picture of the direct-current power supply and its application for outputting pulse current. (**b**) A homemade stainless chamber for thermal shock annealing. (**c**) Picture of infrared pyrometer and high-speed data-acquisition workstation for temperature measurement.

The synthesis of Mo_xC were achieved through the employment of a homemade electrical heating setup based on the Joule heating principle. The electrical heating setup was mainly consisting of three systems, including:

(i) **Energy supply system**: We use a Keithley 2260B-80-40 direct-current power supply for programmable-controlled pulse current delivery, capable of a maximum output of 40.5 A/80 V/1080 W. In a typical thermal shock annealing experiment, the target temperature was achieved by adjusting the value of output power.

(ii) **Reaction chamber**: Designed for electricity-triggered high-temperature reactions, this chamber can accommodate various atmospheres such as Ar or N_2 for electricity-triggered high-temperature reactions. During a typical thermal shock annealing process, a carbon cloth/precursor pellet/carbon cloth sandwich structure was fixed to the copper electrodes, and a programmable high-temperature pulse on carbon cloth could be generated by the input of a pulse current.

(iii) **Temperature measurement system**: Temperature variation during the Joule heating are captured by a non-contact infrared pyrometer (IMGA 740, IMPAC), which has a high-speed data-acquisition capability (one temperature point per microsecond) and can accurately measure temperatures ranging from 350 °C to 3500 °C with a very low uncertainty (<0.3%). This precision is vital for monitoring the rapid thermal changes in our thermal shock annealing processes.

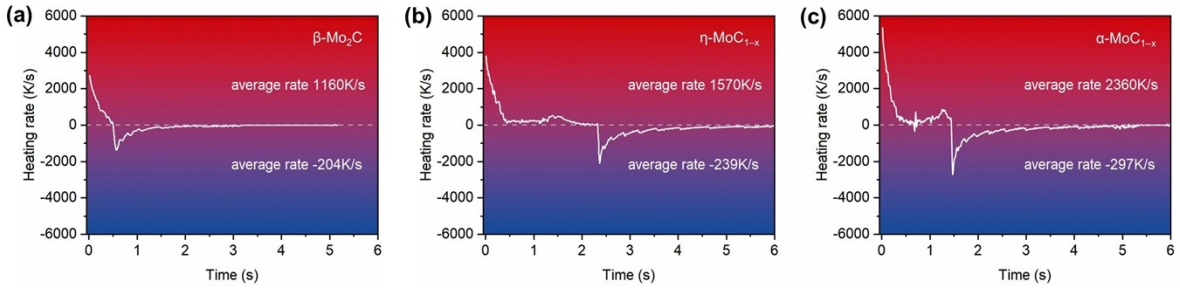

Figure S2. Heating rate-Time curves for the synthesis of β-Mo_2C, η-MoC_{1-x} and α-MoC_{1-x} phase, derived by differentiating the temperature-time curves during the pulsed Joule heating (PJH) process.

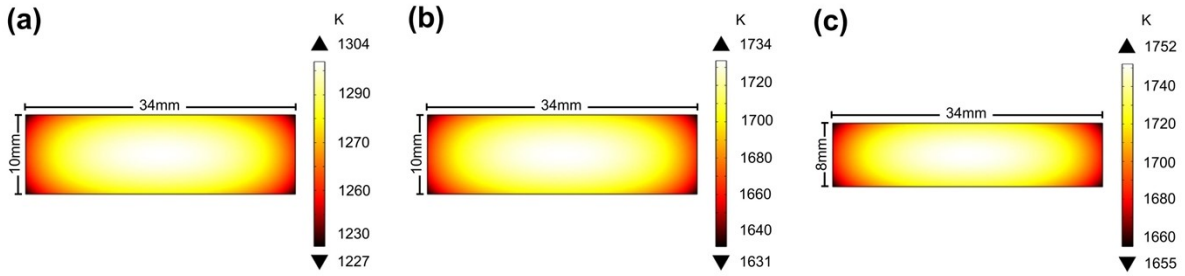

Figure S3. Planar temperature distribution during molybdenum carbide synthesis using COMSOL Multi-Physics simulations. This figure illustrates the temperature distribution across the carbon cloth (CC) layers during the synthesis of different molybdenum carbide phases, as simulated by COMSOL Multi-Physics software: (a) Simulation of temperature distribution at ~1300K in β-Mo_2C synthesis. (b) Temperature distribution at ~1730K in η-MoC_{1-x} synthesis. (c) Simulation of temperature distribution at ~1750K in α-MoC_{1-x} synthesis.

In each simulation, the central area of the CC in contact with the pellet (8 mm diameter for synthesizing β-Mo_2C and η-MoC_{1-x}, 6 mm diameter for synthesizing α-MoC_{1-x}) demonstrates a uniform temperature distribution, with a maximum temperature variation of about 20K. Notably, near the copper electrodes (within a 4 mm range), the temperature exhibits more significant fluctuations, reaching a maximum difference of approximately 100K.

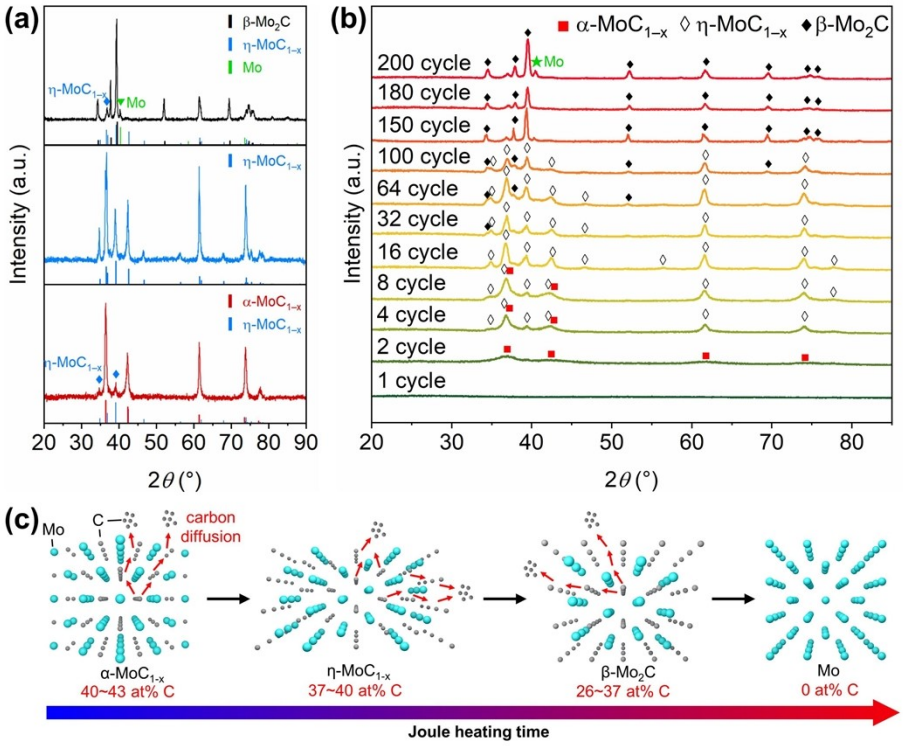

Figure S4. **(a)** XRD patterns of β-Mo_2C (ICDD 00-011-0680), η-MoC_{1-x} (ICDD 01-089-4305) and α-MoC_{1-x} (ICDD 01-089-2868) synthesized by PJH. **(b)** XRD patterns of the intermediate samples in different pulse heating cycles during the PJH process. Pure α-MoC_{1-x}, η-MoC_{1-x} and β-Mo_2C phase are synthesized with different pulse cycles during the continuous pulse heating. **(c)** Schematic of the kinetic process in topotactic transition of molybdenum carbides in "in-outside" processes.

Specifically, the diffraction peaks at 35° and 39.2° in the XRD patterns of α-MoC_{1-x} have been identified as characteristic peaks of η-MoC_{1-x}. Similarly, in the patterns of β-Mo_2C, the peak at 36.6° is identified as a characteristic peak of η-MoC_{1-x}, and the peak at 40° as Mo metal.

The dynamic changes observed in the samples synthesized under different pulse heating cycles have been elaborated upon. The findings suggest that as the number of pulse heating cycles

increases, carbon species diffuse from the bulk to the surface, leading to a gradual decrease in carbon content in the Mo-C system. This process drives the topotactic transition from α-MoC_{1-x} to η-MoC_{1-x} and then to β-Mo_2C, and ultimately to Mo metal (0 at% C).

Addressing the challenges in synthesizing pure phases, the limitations posed by the minimum output time of the current direct-current power supply (500 ms) are acknowledged. A power supply with a shorter minimum output time could enhance the ability to synthesize single-phase α-MoC_{1-x} and β-Mo_2C with higher purity.

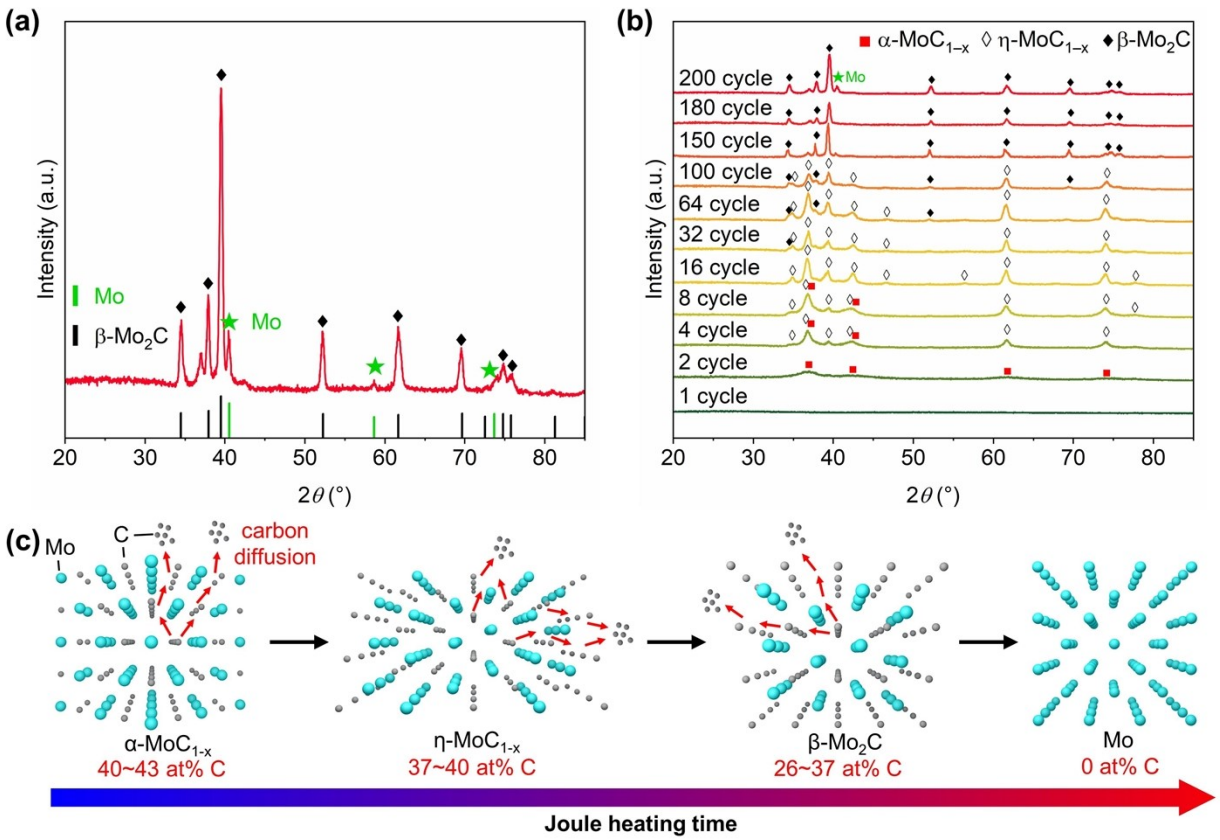

Figure S5. (a) XRD pattern of the products synthesized by 200 cycles. **(b)** XRD patterns of the intermediate samples in different pulse heating cycles during the PJH process. **(c)** Schematic of the kinetic process in topotactic transition of molybdenum carbides in "in-outside" processes.

This transformation was observed over a range of heating cycles: α-MoC_{1-x} was synthesized at 1 cycle, η-MoC_{1-x} at 16 cycles, and β-Mo_2C at 150 cycles, all at a peak temperature of ~1300 K. To further elucidate this transformation, XRD analysis was conducted on products synthesized after 180 and 200 cycles. The results, shown in Figures S5a and S5b, indicate that the product after 200 cycles exhibits diffraction peaks characteristic of Mo metal at 41°.

This progression highlights that as the number of pulse heating cycles increases, carbon species diffuse from the bulk to the external surface, driving a continuous reduction in carbon content. This leads to a topotactic transition from α-MoC_{1-x} to η-MoC_{1-x}, then to β-Mo_2C, and ultimately to metallic Mo (0 at% C). Figure R5c has been updated with a schematic illustration to provide a clearer understanding of the kinetic process in these "inside-out" topotactic transitions.

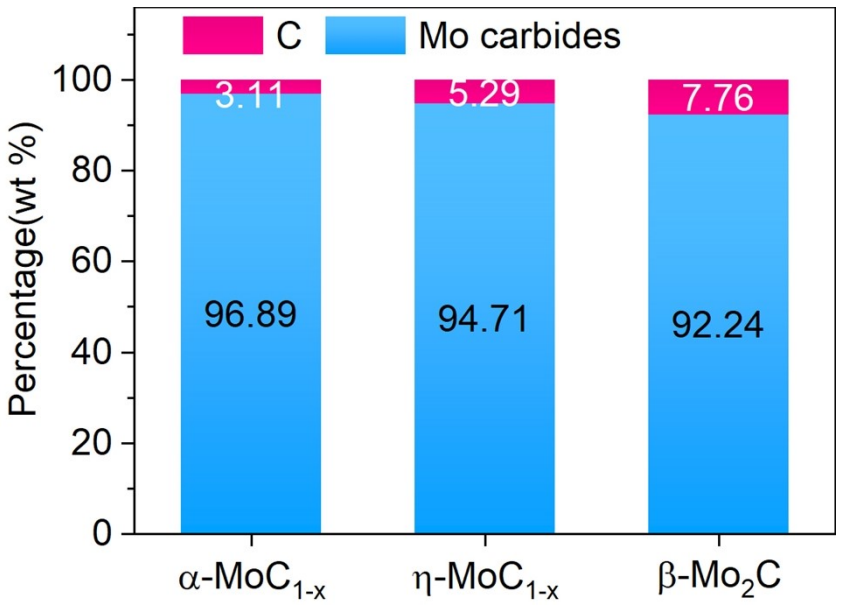

Figure S6. Analysis of molybdenum carbides and carbon content in products via ICP-OES. The Molybdenum carbides content of products is decreasing continuously while the carbon content is creasing in Mo-C system as the carbon species diffuse continuously from the bulk to the external surface.

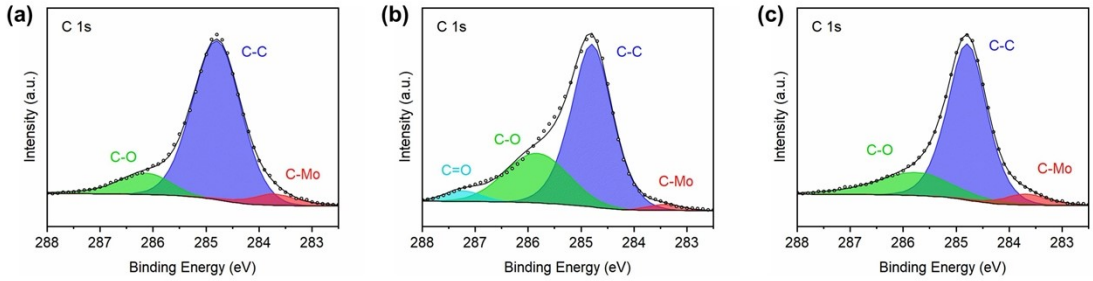

Figure S7. X-ray photoemission spectroscopy (XPS) spectra of (a) α-MoC_{1-x}, (b) η-MoC_{1-x} and (c) β-Mo_2C. In each spectrum, the characteristic Mo-C peak is evident within the C 1s core-level spectra, showcasing the presence of molybdenum-carbide bonds across all three phases.

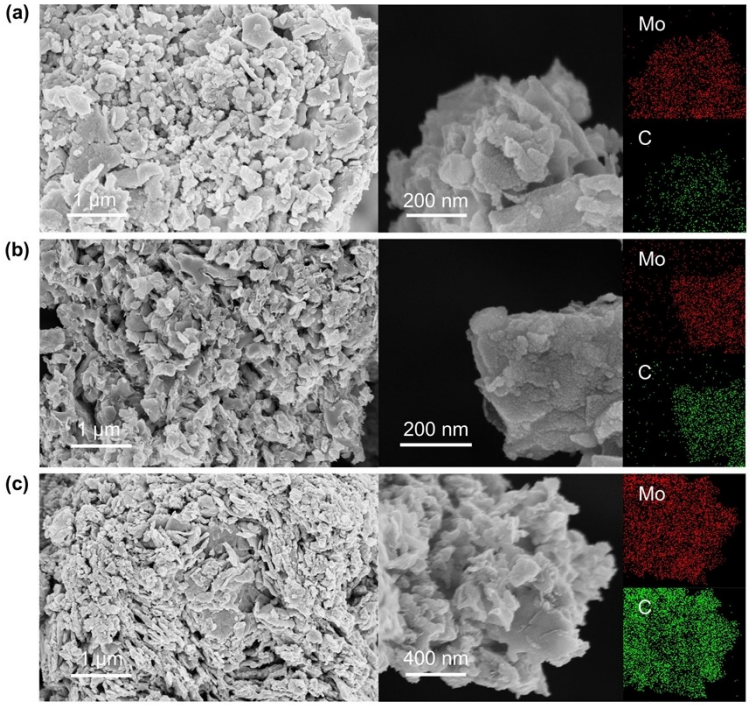

Figure S8. Scanning electron microscopy (SEM) images and energy dispersive spectroscopy (EDS) mapping of (a) β-Mo_2C, (b) η-MoC_{1-x}, (c) α-MoC_{1-x} samples.

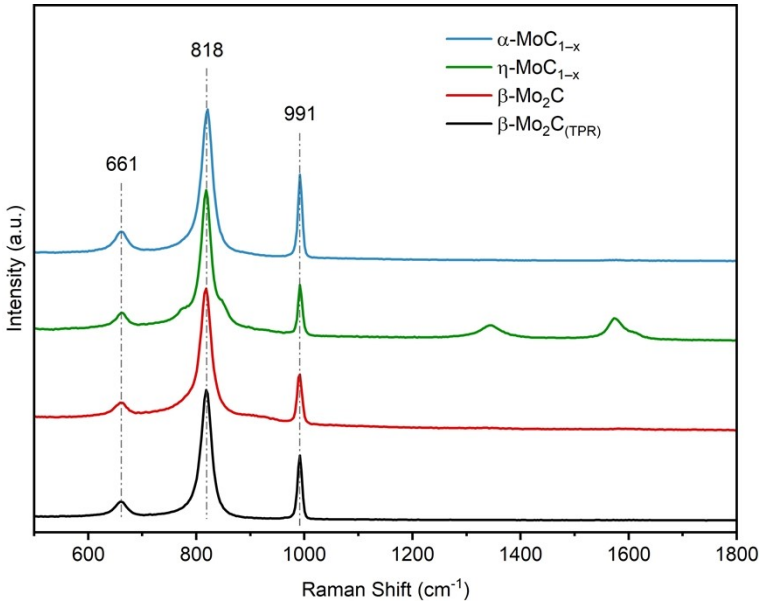

Figure S9. Raman spectra for the three different phases of molybdenum carbides.

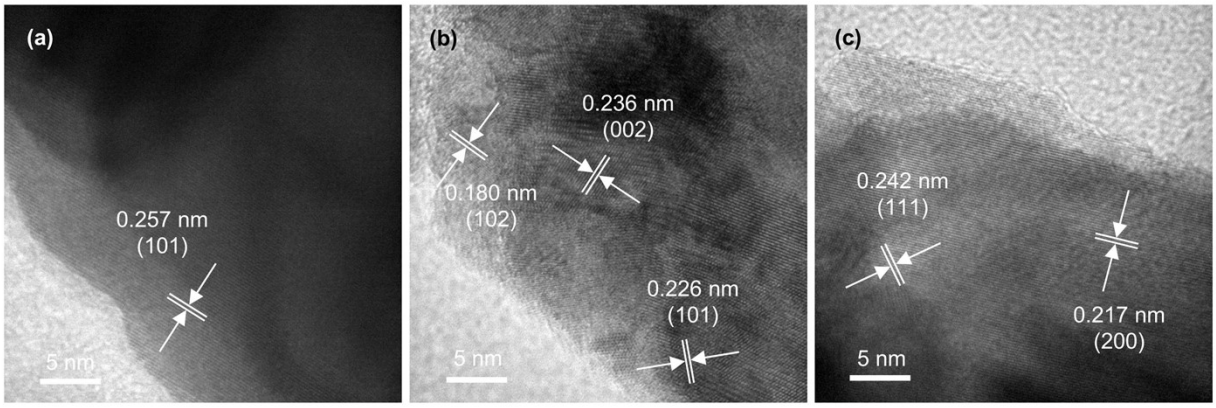

Figure S10. High-resolution transmission electron microscopy (HRTEM) images of (a) β-Mo_2C, (b) η-MoC_{1-x}, (c) α-MoC_{1-x}.

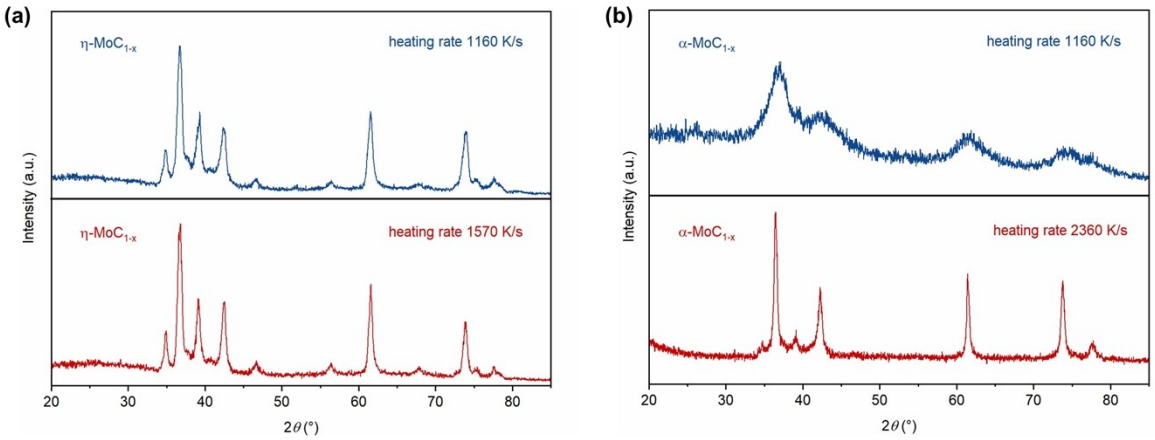

Figure S11. (a) XRD patterns of η-MoC_{1-x} phase synthesizing by average heating rate 1160 K/s and 1570 K/s. (b) XRD patterns of α-MoC_{1-x} phase synthesizing by average heating rate 1160 K/s and 2360 K/s.

The XRD patterns reveal that the η-MoC_{1-x} phase synthesized at the higher heating rate of 1570 K/s exhibits sharper characteristic peaks compared to the phase synthesized at 1160 K/s, suggesting enhanced crystallinity at the higher heating rate. Similarly, the α-MoC_{1-x} phase synthesized at an even higher rate of 2360 K/s shows significantly better crystallinity than the phase produced at 1160 K/s, further corroborating the impact of heating rate on the crystalline quality of these molybdenum carbide phases.

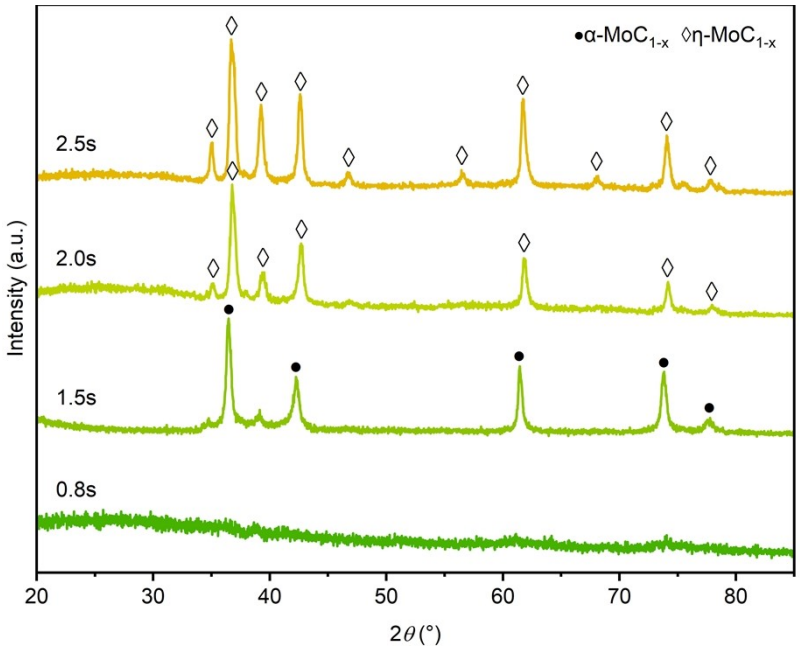

Figure S12. XRD patterns of products by PJH with 30 A, 1 cycle and different pulse time using MoO_x/4-Cl-o-phenylenediamine hybrid as the precursor.

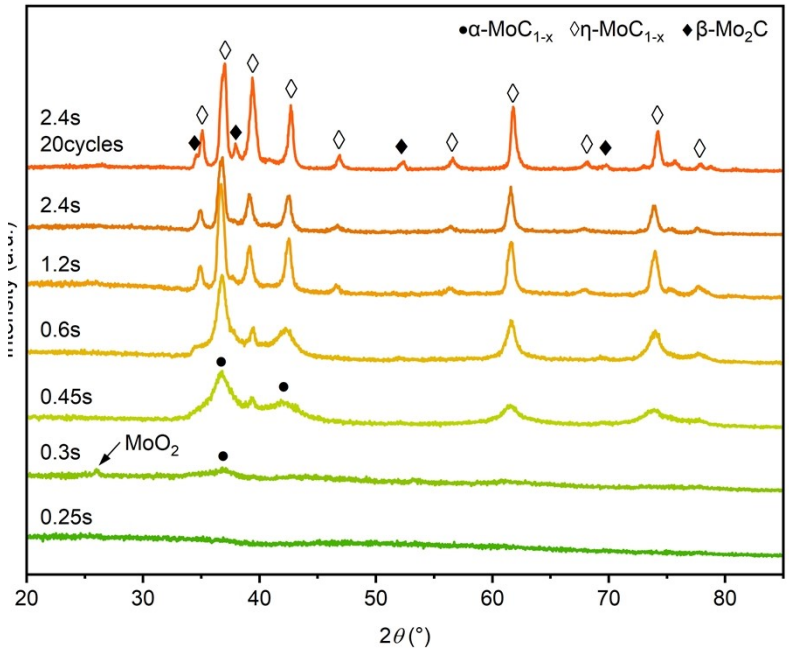

Figure S13. XRD patterns of products by PJH with 34 A, 4 cycles/20 cycles and different pulse time using MoO_x/4-Cl-o-phenylenediamine hybrid as the precursor.

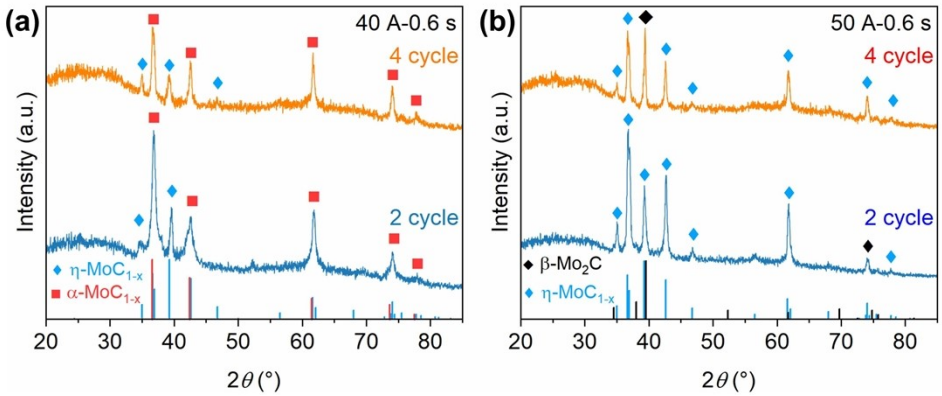

Figure S14. (a) XRD patterns of products by PJH with 40 A, 0.6 s and different pulse cycle. (b) XRD patterns of products by PJH with 50 A, 0.6 s and different pulse cycle.

In addition to the direct-current power supply used in the method, we have also tried to use another direct-current power supply with a higher limit power (IT6532D, Itech Electronic Co., Ltd. The maximum output current/voltage/power is 240 A/80 V/6 KW) to try to synthesize Mo_xC. As shown in Figure S14a, the intensity of the diffraction peak of η-MoC_{1-x} observed at 35°, 39.2° and 46.7 degrees in XRD patterns has increased after 4 cycles with PJH at 40 A current lasting 0.6 s, compared to that after 2 cycles. η-MoC_{1-x} was synthesized by 2 cycles with PJH at 50 A current lasting 0.6 s, then the intensity of the diffraction peak of β-Mo_2C observed at 39.5° in XRD patterns has increased obviously after 4 cycles (Figure S14b). These results confirm that the topotactic transition from α-MoC_{1-x} to η-MoC_{1-x} and then to β-Mo_2C is achievable even under conditions of higher peak temperatures.

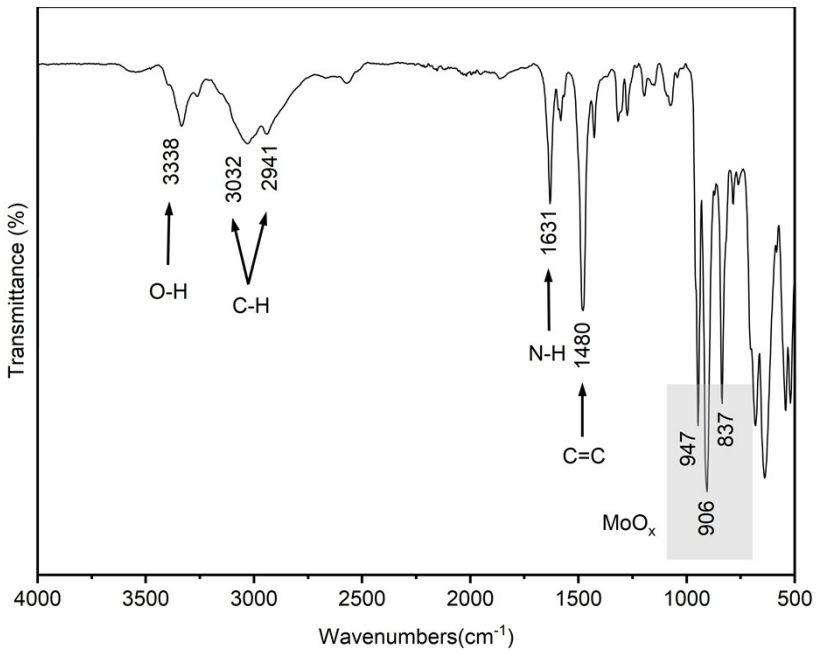

Figure S15. FTIR spectra of MoO_x/4-Cl-o-phenylenediamine hybrid.

The FTIR spectra shows the characteristic absorption bands of 4-Cl-o-phenylenediamine centered at 3032, 2941, 1631, 1480 cm^{-1} and of molybdate at 947, 906 and 837 cm^{-1}, confirming the incorporation of the organic and the inorganic components in the precipitates.

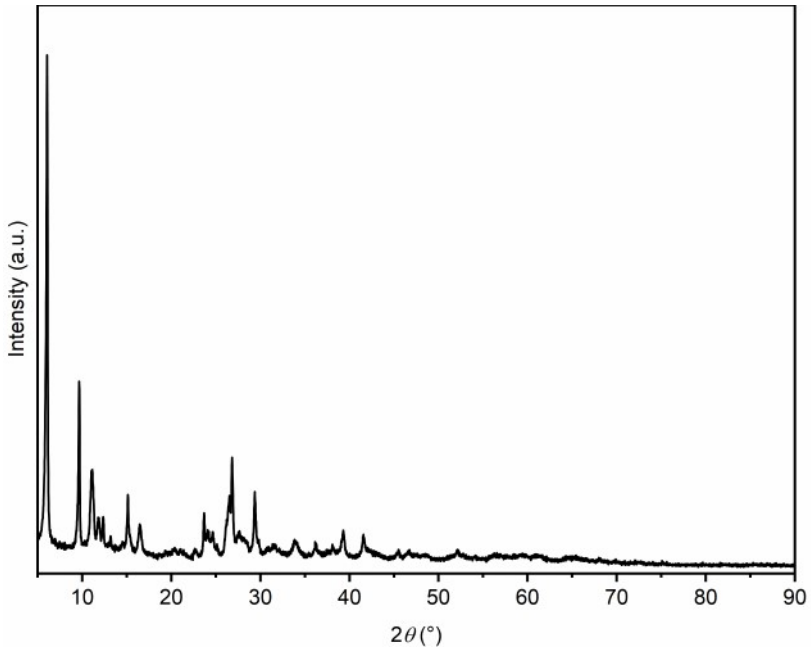

Figure S16. XRD pattern of MoO_x/4-Cl-o-phenylenediamine hybrid.

The XRD spectra of MoO_x/4-Cl-o-phenylenediamine hybrid reference materials have not been reported yet. However, its XRD pattern shows the typical characteristic diffraction peaks in low angle range as other MoO_x/amine hybrid in the previous report.[2]

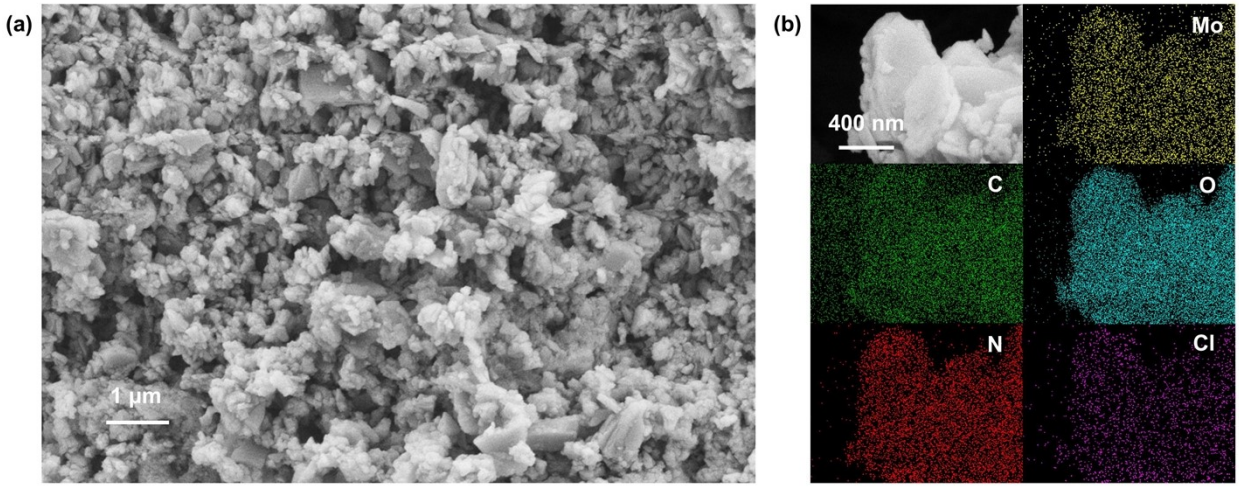

Figure S17. (a) Scanning electron microscopy (SEM) image of MoO_x/4-Cl-o-phenylenediamine hybrid. (b) Energy dispersive spectroscopy (EDS) mapping of MoO_x/4-Cl-o-phenylenediamine hybrid.

The SEM image reveals the presence of nanoplates with varying sizes in the MoOx/4-Cl-o-phenylenediamine hybrid sample. The EDS elemental mapping illustrates the uniform distribution of Mo, C, O, N, and Cl elements within the hybrid. Notably, the carbon element is also detected outside the sample area, which is attributed to the sample powder being placed on conductive adhesive during the analysis. Those observations, combined with the FTIR spectra (Figure S11) and XRD pattern (Figure S12), confirm the successful synthesis of the MoOx/4-Cl-o-phenylenediamine hybrid. These observations indicate that the hybrid was formed through a chemical reaction between molybdate and 4-Cl-o-phenylenediamine, rather than mere physical mixing, showcasing its well-defined compositional and structural attributes.

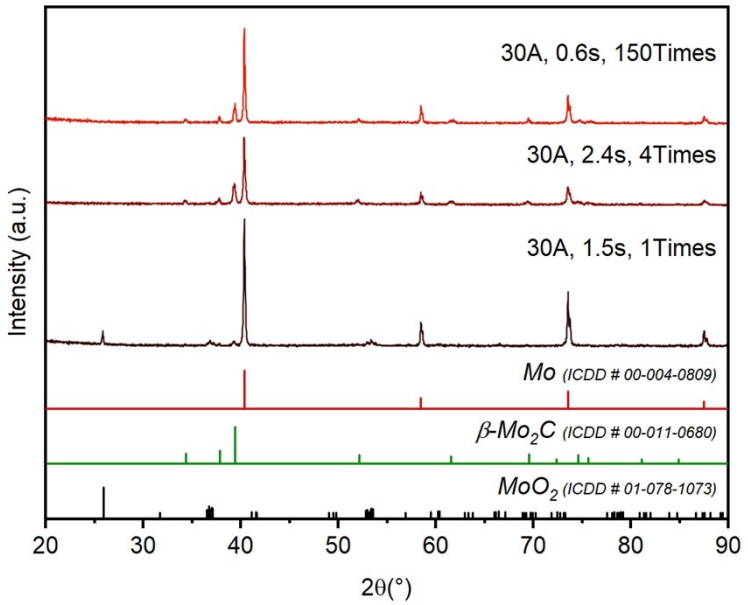

Figure S18. XRD patterns of products obtained through PJH using a physical mixture of ammonium paramolybdate tetrahydrate and 4-Cl-o-phenylenediamine as the precursor.

The XRD analysis reveals a predominant reduction of molybdate to metallic Mo in the products synthesized with this physical mixture. A smaller proportion is reduced to molybdenum oxide, which subsequently reacts with the carbon source to form β-Mo_2C. These findings underscore the crucial role of the hybrid precursor in facilitating the efficient synthesis of molybdenum carbides, as opposed to the limited effectiveness of a mere physical mixture of reactants.

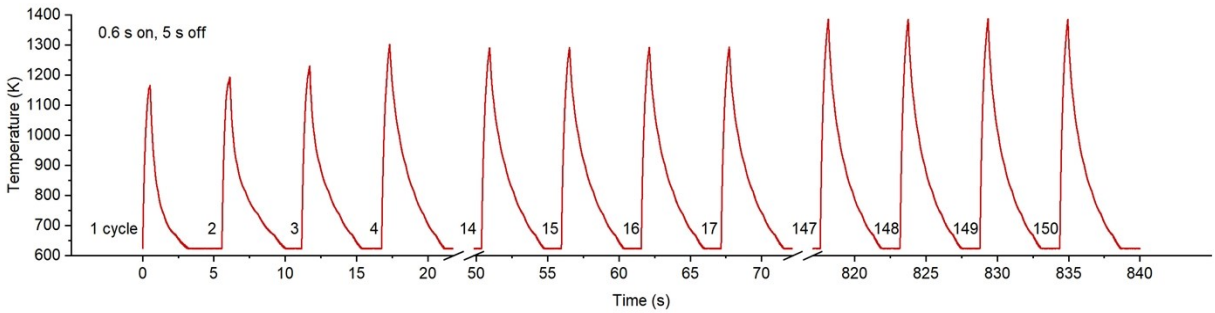

Figure S19. Temperature-Time curve of synthesizing molybdenum carbides by PJH with different numbers of pulse heating cycles.

In the initial three cycles, the rate of temperature rise exhibits notable fluctuations. These variations are likely linked to the thermal reactions occurring within the MoO_x/4Cl-oPDA hybrid. Additionally, a slight increase in temperature (around 50 K) is observed after 100 cycles, which could be attributed to changes in the electrical conductivity of the carbon cloth (CC) due to prolonged electrification.

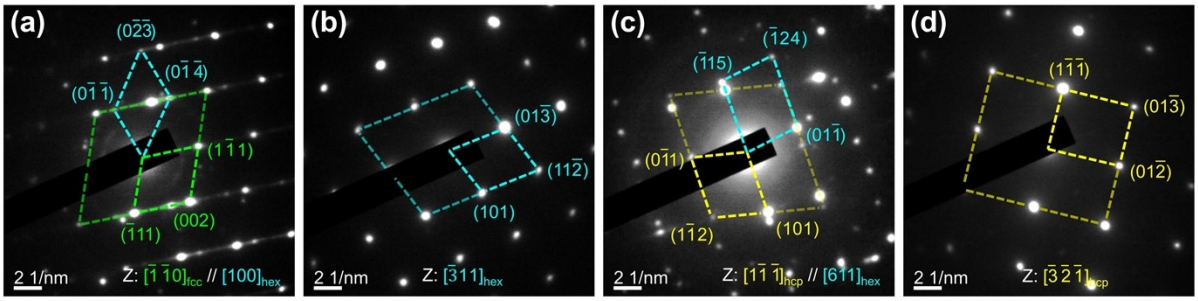

Figure S20. SAED pattern obtained on (a) the intermediate between α-MoC_{1-x} and η-MoC_{1-x}. (b) single η-MoC_{1-x} phase. (c) the intermediate between η-MoC_{1-x} and β-Mo_2C. (d) single β-Mo_2C phase.

The crystal structures of single Mo_xC phase and intermediates are all confirmed by selected area electron diffraction (SAED) patterns. As shown in Figure R8a, the SAED analysis confirmed the presence of both α-MoC_{1-x} and η-MoC_{1-x} in the sample, as evidenced by the distinct diffraction patterns corresponding to each phase. Similarly, Figure R8c displayed separate sets of diffraction spots indicative of η-MoC_{1-x} phase and β-Mo_2C phase. Single η-MoC_{1-x} phase (**Figure R8b**) and single β-Mo_2C phase (**Figure R8d**) in other stages of the synthesis process was substantiated by SAED patterns. These results also indicate a phase transformation from α-MoC_{1-x} to η-MoC_{1-x} and then to β-Mo_2C.

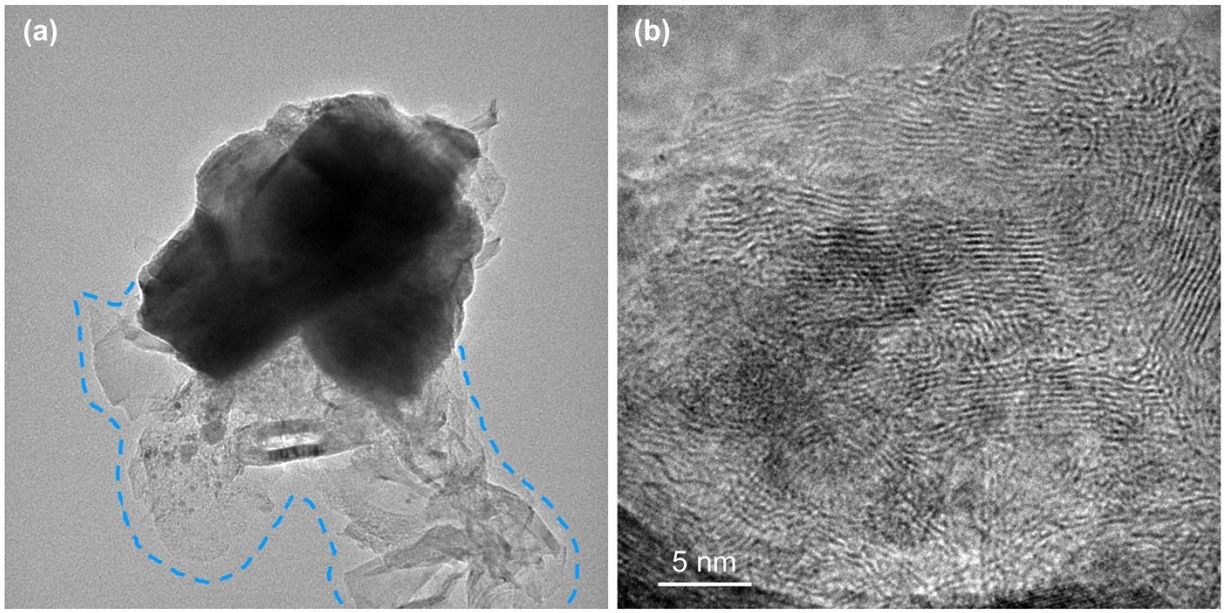

Figure S21. TEM images of molybdenum carbide.

Carbon diffusing from the bulk can be found near molybdenum carbide crystals obviously, which has a tendency of graphitization.

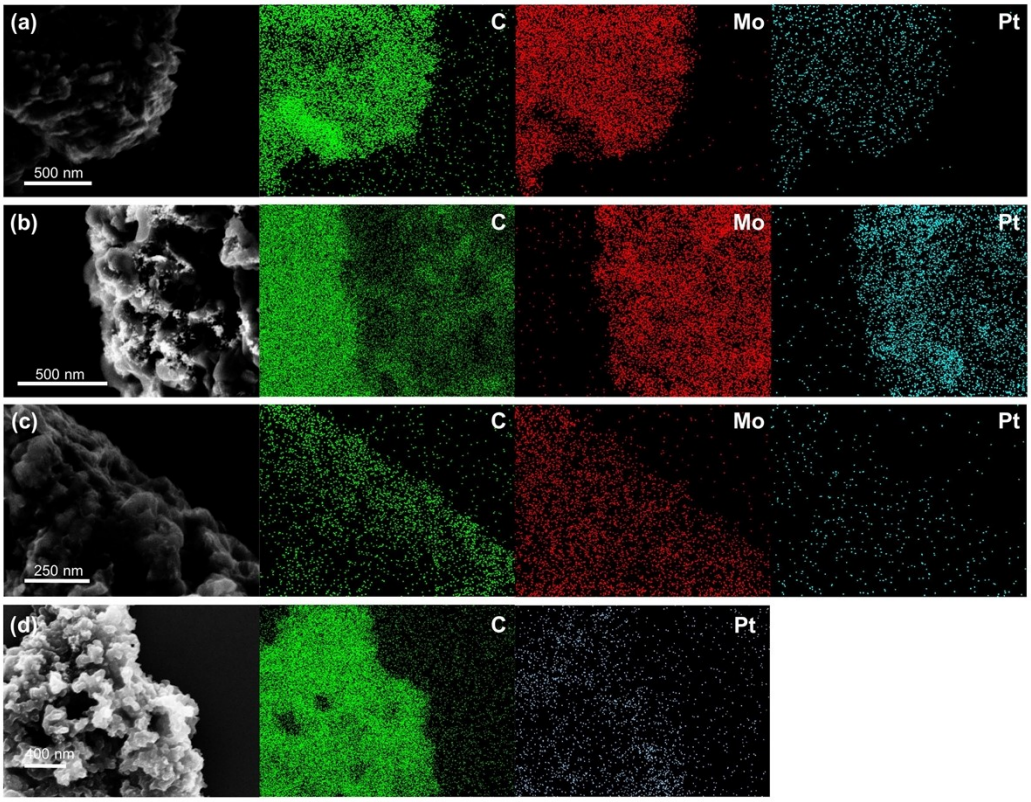

Figure S22. SEM images and corresponding EDS elemental mapping images of three Pt modified molybdenum carbides and Pt/C

The corresponding EDS elemental mapping images show uniform distribution of Mo, C and Pt.

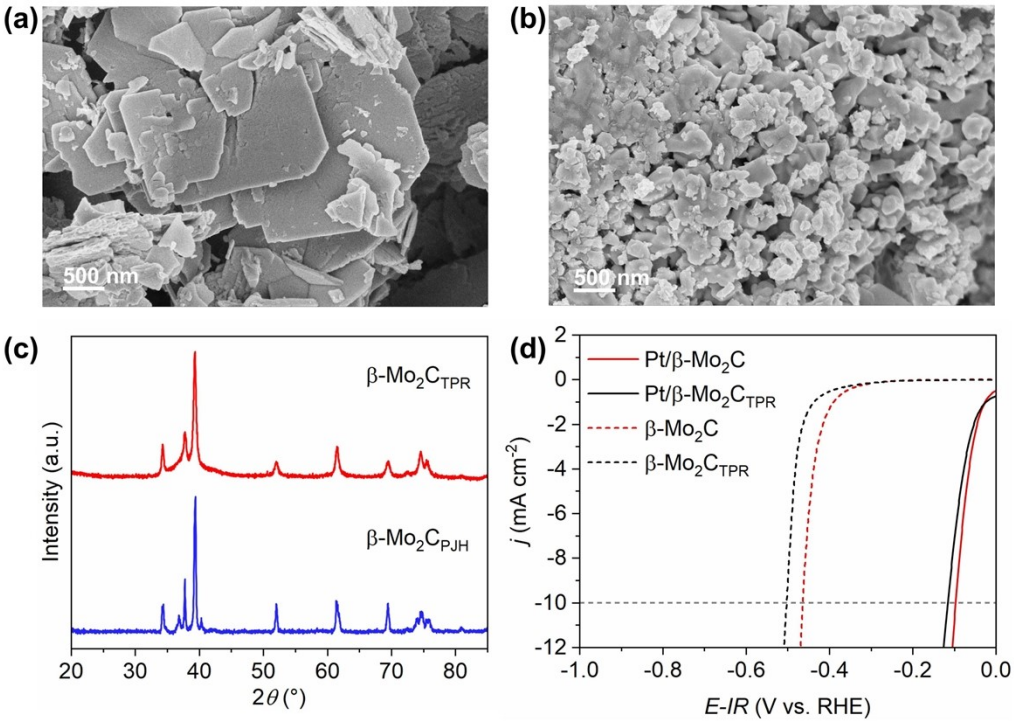

Figure S23. SEM image of (a) β-Mo_2C_{TPR} and (b) β-Mo_2C_{PJH}. (c)XRD patterns of β-Mo_2C_{TPR} and β-Mo_2C_{PJH}. (d) HER polarization curves of β-Mo_2C before and after Pt modification. The β-Mo_2C_{TPR} obtained from temperature-programmed reduction (TPR) was used as a control.

The molybdenum carbide particles synthesized via the PJH method are smaller and more catalytically effective compared to those prepared by temperature-programmed reduction (TPR). The morphology of β-Mo_2C_{TPR} synthesized through TPR typically forms large flakes due to prolonged thermal treatment (Figure S23a). In contrast, the β-Mo_2C_{PJH} particles produced by the PJH method are significantly smaller, attributed to the short heating time and rapid heating/cooling rates, which kinetically inhibit the coarsening or agglomeration of the molybdenum carbide crystals (Figure S23b). Therefore, β-Mo_2C_{PJH} particles synthesized by the PJH method have a larger specific surface area, enhancing their catalytic efficacy. For instance,

the catalytic performance of β-Mo_2C_{PJH} synthesized by PJH surpasses that of β-Mo_2C_{TPR} synthesized via TPR in HER (Figure S23d).

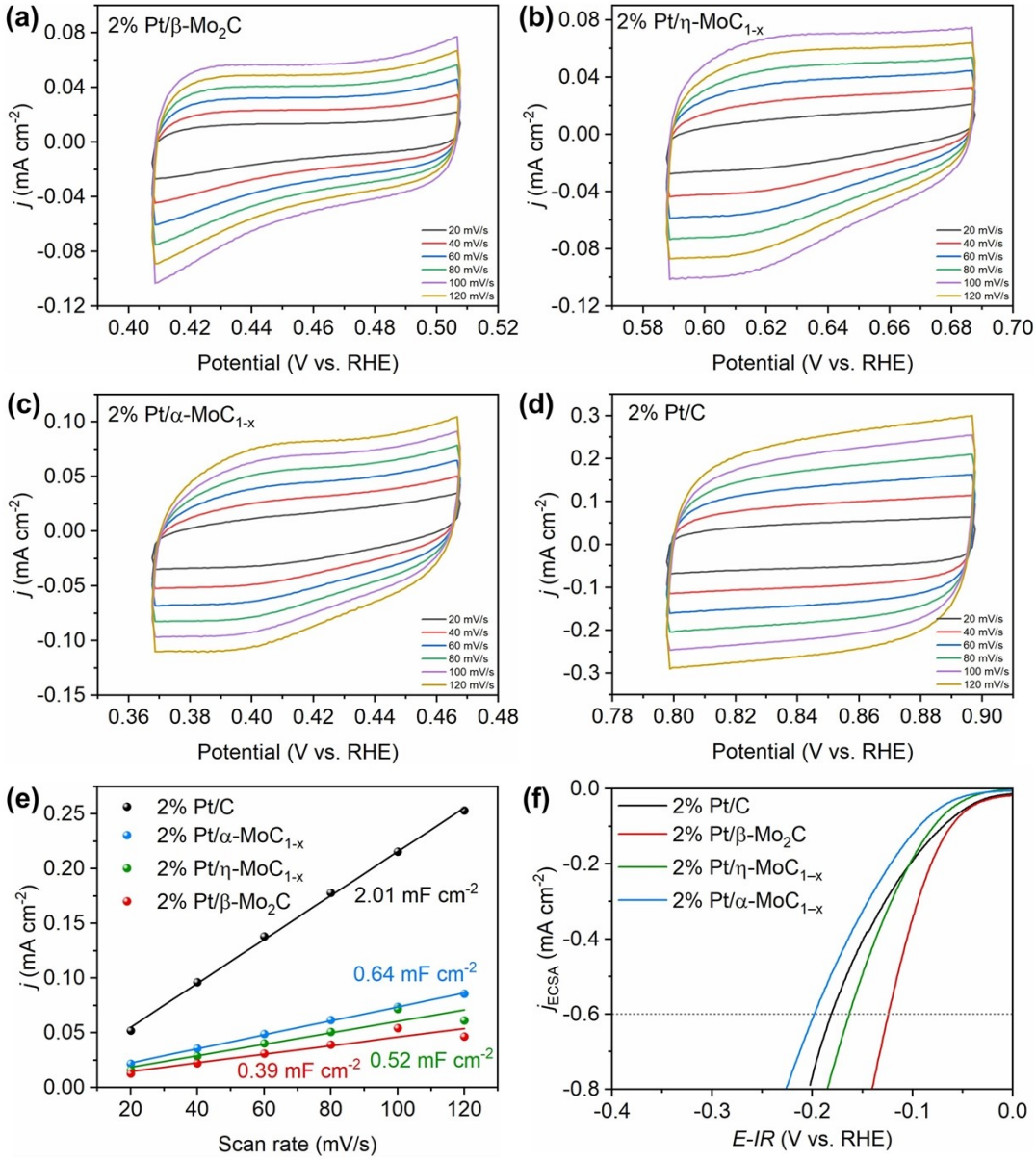

Figure S24. Cyclic voltammograms of **(a)** 2% Pt/*β*-Mo_2C, **(b)** 2% Pt/*η*-MoC_{1-x}; **(c)** 2% Pt/*α*-MoC_{1-x}; **(d)** 2% Pt/C with various scan rates in 0.5 M H_2SO_4. **(e)** The double-layer charging currents at the non-Faradaic potential region were plotted against the scan rate to calculate the double-layer capacitance. The linear fit demonstrates the capacitance values at different scan rates. **(f)** Polarization curves of three phases of molybdenum carbides and molybdenum carbides supported Pt in HER. The current densities of these catalysts were normalized by

electrochemically active surface areas (ECSAs). The 2% Pt/C catalyst synthesized by the same incipient wetness impregnation (IWI) was used as a control.

The current densities of these catalysts were normalized by ECSA in HER (**Figure R14f**). Linear scan voltammetry (LSV) curves revealed that the 2 % Pt/β-Mo_2C, 2 wt% Pt/η-MoC_{1-x} and 2 wt% Pt/α-MoC_{1-x} required the overpotential ($\eta_{j\mathrm{ECSA}0.6}$) versus a reversible hydrogen electrode (RHE) of –124, –163 and –198 mV, respectively, highlighting different effects of three molybdenum carbide phases on the electronic properties of Pt. Notably, the HER activity of the 2% Pt/ C catalyst was lower than that of 2 % Pt/β-Mo_2C and 2 wt% Pt/η-MoC_{1-x}, which highlights the beneficial effects of electronic metal-support interaction (EMSI) via electron transfer from Mo to Pt in boosting the HER activity. The facilitated electron transfer/proton donation achieved through the EMSI between Pt and the Mo_xC support is beneficial to the more facile proton adsorption and desorption on Pt/Mo_xC than Pt/C.[3]

The HER activity of the 2% Pt/α-MoC_{1-x} catalyst was lower than that of 2 % Pt/ C, which could due to the transfer of electrons from platinum to α-MoC_{1-x} leads to the slower HER kinetics of Pt/α-MoC_{1-x}.[4] It is crucial to emphasize that the hydrogen evolution reaction (HER) activity tests are mainly used to demonstrate the structure-activity relationships of different molybdenum carbide-supported platinum catalysts. Employing various molybdenum carbides as carriers to modulate electronic metal-support interaction is of significant importance for designing targeted catalysts based on the electronic structure requirements dictated by the catalytic reactions.

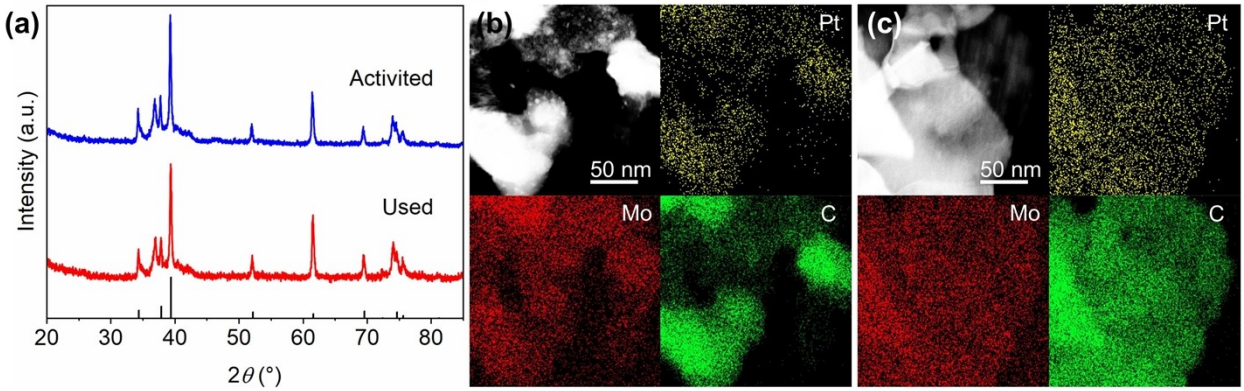

Figure S25. (a) XRD pattern of fresh Pt/β-Mo_2C and used Pt/β-Mo_2C. EDS elemental mapping images of Pt/β-Mo_2C (b) before and (c) after HER stability test.

The β-Mo_2C crystal structure was consistent after HER stability test, and Mo, C and Pt elements were all evenly distributed even after the test.

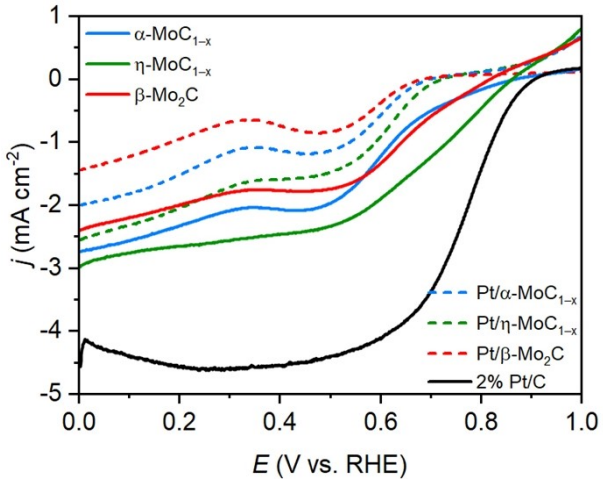

Figure S26. Polarization curves of three phases of molybdenum carbides and molybdenum carbides supported Pt in ORR.

REFERENCES

1 G. Ragoisha and Y. Aniskevich, *Journal of Solid State Electrochemistry*, 2021, **25**, 753-753.

2 Q. S. Gao, C. X. Zhang, S. H. Xie, W. M. Hua, Y. H. Zhang, N. Ren, H. L. Xu and Y. Tang, *Chemistry of Materials*, 2009, **21**, 5560-5562.

3 D. S. Baek, G. Y. Jung, B. Seo, J. C. Kim, H.-W. Lee, T. J. Shin, H. Y. Jeong, S. K. Kwak and S. H. Joo, *Advanced Functional Materials*, 2019, **31**, 1804690.

4 L. L. Lin, W. Zhou, R. Gao, S. Y. Yao, X. Zhang, W. Q. Xu, S. J. Zheng, Z. Jiang, Q. L. Yu, Y. W. Li, C. Shi, X. D. Wen and D. Ma, *Nature*, 2017, **544**, 80-83.